This article has been accepted for publication in IEEE Internet of Things Journal. This is the author's version which has not been fully edited and content may change prior to final publication. Citation information: DOI 10.1109/JIOT.2024.3470321

Wi-Pulmo: Commodity WiFi Can Capture Your Pulmonary Function Without Mouth Clinging

Peng Zhao[1], Jinyang Huang[1*], Xiang Zhang*, Zhi Liu, Huan Yan, Meng Wang, Guohang Zhuang, Yutong Guo, Xiao Sun, and Meng Li

***Abstract*—Pulmonary function testing is a crucial examination for respiratory diseases. Current medical spirometers are bulky and inconvenient, while available portable spirometers are extremely expensive and often lack accuracy. Furthermore, both devices require direct contact, inevitably increasing the cross-infection risk. To tackle these challenges, we propose *Wi-Pulmo*, an end-to-end deep learning-based *Wireless System* that utilizes WiFi channel state information (CSI) to provide contact-free, convenient, cost-effective, and precise *Pulmonary* Function Testing outside the clinical setting. Based on the analysis of thoracic and abdominal movement patterns, *Wi-Pulmo* first validates the feasibility of using WiFi to estimate pulmonary function. Then, *Wi-Pulmo* designs an efficient fine-grained sensing quality-based algorithm for complete exhalation segmentation. Additionally, a relevant interference-tolerant learning algorithm based on Variational Inference is proposed to accurately map the CSI of WiFi signals to pulmonary function. Extensive experiments achieved average monitoring error rates of 2.59% for normal subjects in daily scenarios and 5.87% for real patients in tertiary hospitals over a two-month period. These satisfactory results demonstrate the strong effectiveness and robustness of *Wi-Pulmo*. Furthermore, our findings in clinical reveal a close correlation between chronic diseases and pulmonary function.**

***Index Terms*—WiFi sensing, pulmonary function, the elderly, variational encoder-decoder (VED) network**

I. Introduction

Respiratory diseases, including chronic obstructive pulmonary disease (COPD), bronchial asthma, tuberculosis, lung cancer, pulmonary fibrosis, and pulmonary hypertension, are both common and widespread. Furthermore, inadequate lung function development is linked to increased prevalence and earlier onset of respiratory, cardiovascular, and metabolic diseases, which contributes to premature mortality [1]. In the diagnostic, Pulmonary Function Testing (PFT) is acknowledged as the gold standard for chronic airway diseases. It assesses the parameters such as spirometry, respiratory rate, and expiratory flow rate, serving as a crucial method for evaluating pulmonary function. Fig. 1 illustrates two types of spirometers, which are the most common instruments employed for PFT. Although medical spirometers provide precise and comprehensive results, their use is restricted to hospital settings due to the bulky equipment and cumbersome procedures involved. Additionally, portable spirometers, while convenient for patients, are often expensive and prone to higher error rates (usually $\geq 20\%$ error [2]). Furthermore, both types of devices necessitate human contact, thereby elevating the risk of cross-infection.

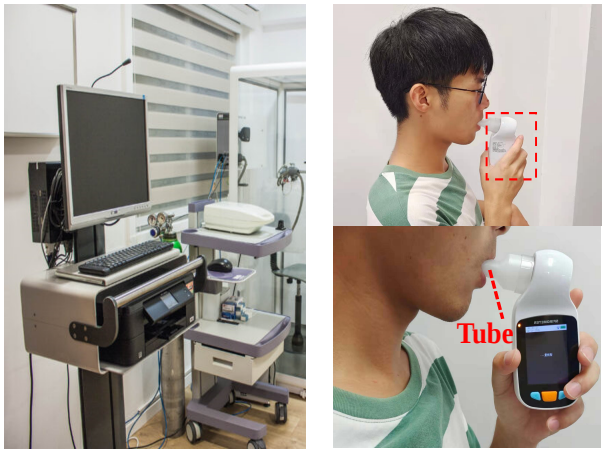

(a) Medical spirometer. (b) Portable spirometer.

Fig. 1: Spirometers used in clinic and home.

Therefore, ensuring daily PFT is contact-free, convenient, accurate, and cost-effective remains challenging. In addition to directly measuring pulmonary function with spirometry, indirect assessment methods by observing thoracoabdominal movements have gradually attracted the attention of researchers in recent years. A range of sensing technologies shows the potential to be applied for indirect pulmonary function estimation, such as wearable sensors, vision-based sensors, acoustic-based sensors, and radio frequency (RF)-based sensors. Wearable sensors provide [3]–[5] high accuracy, but they usually require contact with the user's body, which may cause discomfort. Vision-based sensors [6]–[10] only work under good lighting conditions and are primarily used to measure respiratory rate. Acoustic methods for measuring pulmonary function are complex. One method requires a special prop and a quiet environment to evaluate changes in acoustic features during exhalation [11]–[14]. Another promising method involves echo-based acoustic sensing, while this approach still necessitates volunteers to handheld a smartphone during the measurement process and has a monitoring error of 5%-10% [15]. Recently, gradually increasing research focusing on RF-based techniques for human respiration monitoring, which is device-free for users [16]–[23]. However, the majority of these studies solely concentrate on the frequency infor-

Peng Zhao, Jinyang Huang, Xiang Zhang, Huan Yan, Meng Wang, Guohang Zhuang, Yutong Guo, Xiao Sun, Meng Li, School of Computer and Information, Hefei University of Technology, Hefei, 230601, China.

Xiang Zhang, and Jinyang Huang, are with CAS Key Laboratory of Electromagnetic Space Information, University of Science and Technology of China, Hefei, 230026, China.

Zhi Liu, Department of Computer and Network Engineering, The University of Electro-Communications, Tokyo, 1828585, Japan.

[1]Equal contribution.

Corresponding author*: Jinyang Huang (Email: hjy@hfut.edu.cn), Xiang Zhang (zhangxiang@ieee.org)

mation of breathing and neglect to investigate other indices present throughout a complete respiratory cycle, which forms the foundation for pulmonary function testing.

Therefore, in this paper, we investigate whether more detailed and accurate respiratory information can be extracted from CSI data. It basically poses three challenges. Firstly, PFT focuses on a single correct ***waveform of inhalation and exhalation*** to calculate the flow rate and volume of respiration, which poses higher demands on our signal processing pipeline compared to extracting respiratory rate from a long sequence of CSI data. Secondly, performing PFT is not an easy task, as individuals must inhale deeply and then exhale forcefully. Subsequent irrelevant movements, such as abdominal rebound, body tilt, or tremors, introduce ***additional motion noise*** into the collected CSI data. This noise is particularly notable when testing elderly individuals with underlying medical conditions since the elderly's breathing is relatively weak, and the corresponding breath signal response is smaller. Finally, it is challenging to directly map processed WiFi signals that contain thoracoabdominal movement to pulmonary function indices. This difficulty arises due to the uncertainty of WiFi signal characteristics in indoor scenarios affected by multipath environments and the intricate correlation between pulmonary function and thoracoabdominal movements [24], [25].

To address the aforementioned challenges, we propose *Wi-Pulmo*, an end-to-end deep learning-based wireless system leveraging WiFi signals for contact-free, convenient, cost-effective, and precise pulmonary function testing. Several key techniques are employed in *Wi-Pulmo* to realize accuracy PFT. First, to capture ***waveform of inhalation and exhalation*** accurately, *Wi-Pulmo* employs a two-step approach. It initially segments each respiration by examining the velocity of amplitude change. Then, it precisely identifies the beginning and end of each respiration by calculating the Error of the Dynamic Phase (EDP) [26]. Further, to address the challenge of ***additional motion noise***, *Wi-Pulmo* utilizes the CSI-ratio model [27] to eliminate random phase differences caused by RF oscillators, which are inherent hardware flaws. We further design an exhalation data segmentation algorithm to remove the noise and detect the exhalation. Finally, based on Variational Inference (VI) [28], *Wi-Pulmo* design a Variational Encoder-Decoder (VED) network [29], [30] to represent the physiological dynamics correlation that describes the complex correlation between pulmonary function and thoracoabdominal movements. Considering limited training data from some subjects and the inability of patients to use clinical-grade spirometers to obtain true values as labels, two training methods are designed, i.e., personalized training and group training, to solve this problem. The specific procedures will be discussed in Section III-D.

Wi-Pulmo is implemented on commodity WiFi devices and evaluated in a simulated home environment with young and healthy participants. Furthermore, following the approval of the Ethics Committee, we also conduct a two-month clinical study in a hospital involving elderly individuals with underlying lung or cardiovascular diseases. Our contributions are summarized as follows:

- We propose *Wi-Pulmo*, an end-to-end deep learning-based Wireless System that utilizes WiFi CSI to provide contact-free, convenient, cost-effective, and precise PFT outside the clinical setting.
- We first design a novel adaptive breathing information filtering and segmentation algorithm to achieve the segmented CSI that contains the users' thoracoabdominal movements. Then, we design a VED network to accurately recover pulmonary function indices under complex data correlation.
- *Wi-Pulmo* yields an average pulmonary function monitoring error of 2.59% in the laboratory environment and 5.87% in the hospital setting, which demonstrates its potential to accomplish daily pulmonary function testing. Furthermore, our study reveals a correlation between pulmonary function and cardiovascular diseases and emphasizes the significance of regular PFT implementation for elderly individuals.

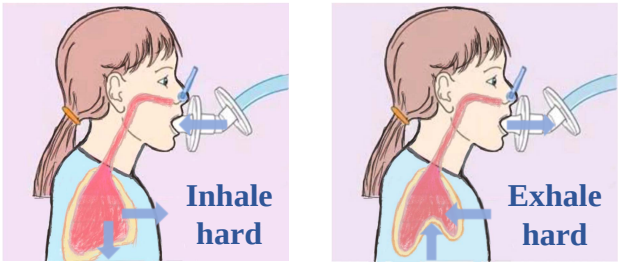

(a) Inspiration. (b) Expiration.

Fig. 2: Two stages included in a standard spirometry.

II. Preliminary

A. Pulmonary Function indices and Spirometry

Pulmonary function testing [31] involves the analysis of several indices of pulmonary function that are measured using specialized instruments. There are numerous indices utilized in pulmonary function tests, with the following being the most commonly used:

- **Forced Vital Capacity (FVC)**: The air volume is exhaled with maximum force and velocity after maximum inspiration. It can be used to diagnose slow branching, small vessels, and emphysema and further evaluate the effectiveness of bronchial extenders.
- **Forced Expiratory Volume in 1 second (FEV1)**: The volume exhaled in the first second after maximum inspiration to total lung volume is an average flow rate measurement for one second. It is the main indicator of impaired pulmonary function.
- **FEV1/FVC**: The ratio of FEV1 to FVC is a meaningful indicator. It is a common index for determining airway obstruction.

As depicted in Fig. 2, the standard spirometry procedure is utilized to evaluate the pulmonary function of patients. It measures the amount of air inhaled, the amount of air exhaled, and the rate of exhalation to comprehensively determine how well the patient's lungs are functioning. This requires subjects to inhale as much air as possible and exhale with maximum effort, and the best duration is more than 6s.

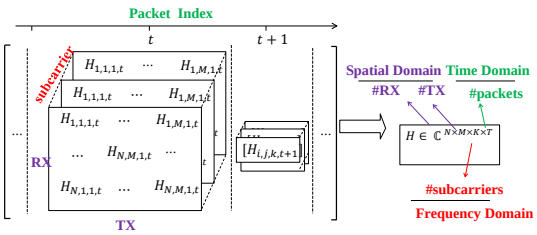

Fig. 3: The format of received CSI data is a 4-dimensional matrix (Number of transmitting antennas × Number of receiving antennas × Number of subcarriers × Time).

B. Channel State Information (CSI)

WiFi CSI plays a crucial role in *Wi-Pulmo*. Fig. 3 represents the channel attribute of the communication link, which describes the attenuation factors of the signal in each transmission path, such as signal scattering, environmental fading, power decay of distance, etc [32]–[34]. Received CSI can be defined as follows [35]–[37]:

$$\boldsymbol{H}(f,t) = \boldsymbol{H}_s(f) + \boldsymbol{H}_d(f,t) + \boldsymbol{\xi}(f,t) \tag{1}$$

The CSI signal can be divided into three components: $\boldsymbol{H}_s(f)$, $\xi(f,t)$, and $\boldsymbol{H}_d(f,t)$. The ***static component*** $\boldsymbol{H}_s(f)$ is the superposition of signals that remain unchanged for a period of time. $\xi(f,t)$ represents ***ambient noise*** [26], which consists of two parts: channel-induced Gaussian noise and dynamic multipath reflected from other moving objects except the chest motion. The most important part of realizing accuracy PFT is $\boldsymbol{H}_d(f,t)$, which contains the ***dynamic component*** reflecting from the chest movement. More specifically, it can be described in the following form:

$$\boldsymbol{H}_d(f,t) = \sum_{n=1}^{N} a_n(f,t) e^{-j2\pi \frac{d_n(t)}{\lambda}} \tag{2}$$

Where n is the total number of propagation paths, f is the frequency for each sub-carrier in multi-path, t is the time stamp, $a_n(f,t)$ is the amplitude attenuation, λ represents the wavelength, and $d_n(t)$ is used to denote the propagation path for n^{th} multi-path component. The dynamic part of the wave that travels along the reflection path of the chest wall with a length of $2\pi d_n(t)$ will experience a shift of $\Delta\varphi(t) = 2\pi \frac{d_n(t)}{\lambda}$. This shift has important implications during the PFT, as $\boldsymbol{H}(f,t)$ will change correspondingly with different respiratory movement status. Theoretically, this allows us to infer the indices of pulmonary function.

C. Spirometry Using CSI

Pulmonary function indices exhibit a close correlation with thoracoabdominal displacement. As shown in Fig 4(a), respiration is a complex physiological behavior involving numerous body parts' coordinated activity. It necessitates the integrated functioning of the respiratory muscles, lungs, and airway passages, all orchestrated by the nervous system to ensure efficient gas exchange. Therefore, in addition to directly measuring and estimating respiratory variables with spirometry, several other techniques and devices relying on the observation of thoracoabdominal displacement have been proposed [24], [38], [39]. Specifically, they analyze the variation pattern of Rib Cage (RB) and thorax and abdomen (ABD) movements to achieve pulmonary function indices indirectly. These thoracoabdominal movements can be further subdivided into four types in Fig. 4(b), including rib cage distance, chest wall distance, abdomen distance, and supine distance. Each variation is considered as Degree Of Freedom (DOF), and we show the formulation of tidal volume (V_T) based on the number of DOF as follows:

$$V_T = \alpha \cdot D_{RC} + \beta \cdot D_{AB} \tag{3}$$

$$V_T = \alpha \cdot D_{RC} + \beta \cdot D_{AB} + \gamma \cdot D_X \tag{4}$$

$$V_T = \alpha \cdot D_{RC} + \beta \cdot D_{AB} + \gamma \cdot D_X + \zeta \cdot D_{PO} \tag{5}$$

where D_{RC}, D_{AB}, D_X and D_{PO} represent the variation distance of the RC, ABD, the displacement between the xiphoid and the umbilicus and the axial displacement of the spine. α, β, γ and ζ are the volume-motion coefficients. Eq (3), (4), (5) represent different numbers of DOF respectively. Respiratory Inductance Plethysmography (RIP), which measures the movement of the chest and abdominal wall during breathing, is a typical method based on 2DOF. RIP is common and effective in monitoring breathing. This method assesses pulmonary ventilation and provides information about pulmonary function [24]. The above analysis presents us with a complex physiological dynamics correlation model between thoracoabdominal movements and lung function. Fortunately, due to the multipath effect in WiFi signals, when the user performs the PFT, the chest wall and abdomen movements will be recorded in the CSI data. These conditions ensure the reliability of using WiFi to measure pulmonary functions.

Further research is needed to investigate the feasibility. As shown in Fig. 5(a), we collect complete PFT data for analysis. In Fig. 5(b), it can be observed that the CSI data contains not only amplitude information but also phase information. However, the amplitude is susceptible to interference, so we choose to utilize the phase information, which offers relatively higher accuracy, for perception. By performing noise elimination, we obtained the data shown in Fig. 5(c) on the complex plane. Finally, through coarse segmentation and fine segmentation using the EDP, we obtained the clean expiratory and inspiratory waveforms depicted in Fig. 5(d). The variations in these waveforms align with chest wall movements, indicating that chest wall motion data can be extracted from the CSI.

III. System Design

A. System Overview

Fig. 6 illustrates the workflow of the *Wi-Pulmo* system. In the initial stage, as depicted in Fig. 6(a), volunteers undergo PFT while *Wi-Pulmo* collects CSI data through the device. As shown in Fig. 6(b), the raw CSI data serves as the input. Considering the higher stability of phase characteristics in CSI, *Wi-Pulmo* primarily focuses on the variations in the CSI phase. Firstly, the phase difference calibration is employed

This article has been accepted for publication in IEEE Internet of Things Journal. This is the author's version which has not been fully edited and content may change prior to final publication. Citation information: DOI 10.1109/JIOT.2024.3470321

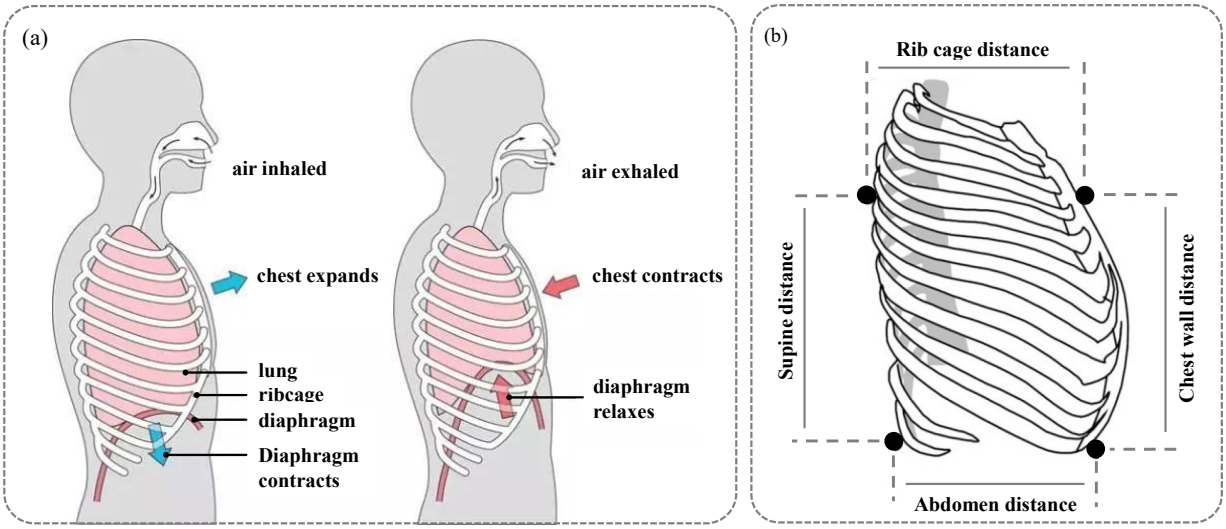

Fig. 4: Breathing mechanics. (a) shows the body parts that vary when a person breathes. (b) shows different 4 degrees of freedom constructed from these body parts [25].

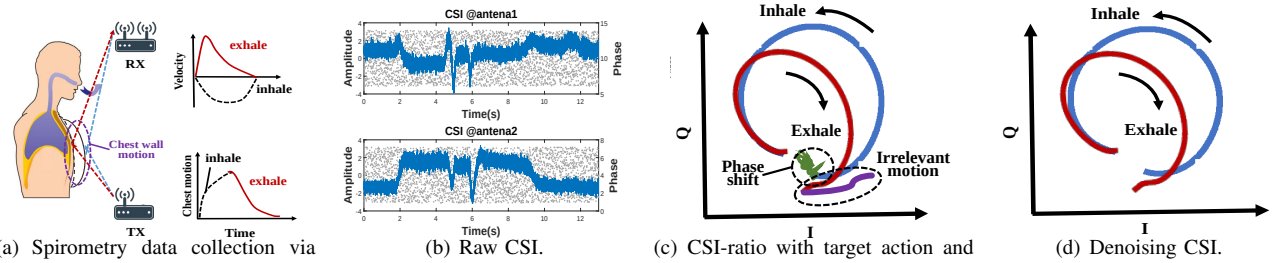

(a) Spirometry data collection via WiFi. (b) Raw CSI. (c) CSI-ratio with target action and noise. (d) Denoising CSI.

Fig. 5: The entire procedure for obtaining data segmentation, including generating thoroughly denoised respiration signals from the raw CSI data.

in *Wi-Pulmo* to remove phase differences introduced by the hardware. Subsequently, the data is fed into the chest wall movement tracking module, where noise elimination, segmentation, and other steps are applied to obtain purified CSI data that only contains chest wall movements. Finally, we propose the VED network to process this data to obtain relevant pulmonary function indices.

B. Phase Offset Remover

For CSI data, due to the lack of synchronization between the transmitter and receiver, each antenna experiences a random phase offset that varies over time. It is illustrated below:

$$\boldsymbol{H}(f,t) = e^{-j\theta}(\boldsymbol{H}_s(f,t) + A(f,t)e^{-j2\pi\frac{d(t)}{\lambda}}), \tag{6}$$

where $e^{-j\theta}$ is the phase offset. As depicted in Fig. 5(b), the presence of this random phase offset hinders our ability to utilize the phase directly. Fortunately, in commodity WiFi devices, different antennas share the same RF oscillator, resulting in consistent random phase offsets. Hence, we can leverage the CSI-ratio model [40] to eliminate this phase offset:

$$\begin{aligned}\boldsymbol{H}_q(f,t) &= \frac{\boldsymbol{H}_1(f,t)}{\boldsymbol{H}_2(f,t)} \\ &= \frac{e^{-j\theta}(\boldsymbol{H}_{s,1} + A_1 e^{-j2\pi\frac{d_1(t)}{\lambda}})}{e^{-j\theta}(\boldsymbol{H}_{s,2} + A_1 e^{-j2\pi\frac{d_2(t)}{\lambda}})} \\ &= \frac{A_1 e^{-j2\pi\frac{d_1(t)}{\lambda}} + \boldsymbol{H}_{s,1}}{A_2 e^{-j2\pi\frac{d_1(t)+\triangle d}{\lambda}} + \boldsymbol{H}_{s,2}}\end{aligned} \tag{7}$$

where $\boldsymbol{H}_1(f,t)$ and $\boldsymbol{H}_2(f,t)$ denote the CSI data received on two antennas. When the antennas are in close proximity, $\triangle d$ is a constant. Applying the Mobius transformation [27], this equation becomes equivalent to translating and rotating $\boldsymbol{H}_1(f,t)$ in the complex plane while preserving the phase variation trend.

After eliminating the random phase offset, a 4-dimensional tensor shown in Fig. 3 is obtained. Fig. 7(a) illustrates a comprehensive PFT on the complex plane, which encompasses the exhalation and inhalation processes. Its shape exhibits two arc-like patterns. However, notable noise is observed in the initial and final segments of the data, which demonstrates the necessity of noise removal. This concern will be addressed in subsequent stages by *Wi-Pulmo*.

This article has been accepted for publication in IEEE Internet of Things Journal. This is the author's version which has not been fully edited and content may change prior to final publication. Citation information: DOI 10.1109/JIOT.2024.3470321

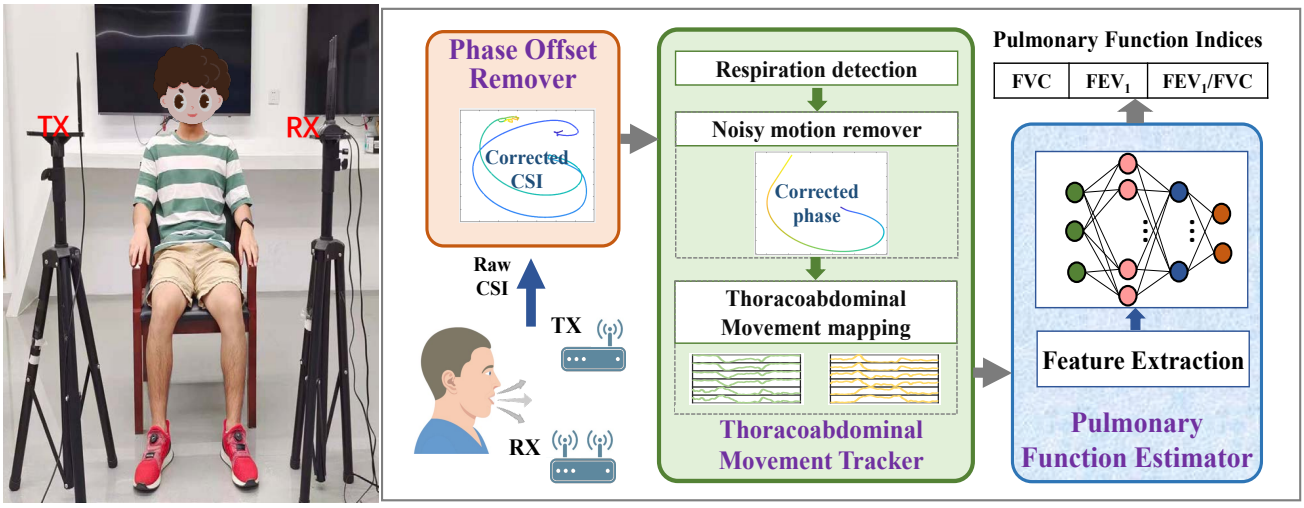

(a) CSI data collection. (b) The system architecture of *Wi-Pulmo*.

Fig. 6: System overview. (a) illustrates the equipment and scenarios used in the collection of CSI data. (b) delineates our comprehensive data processing workflow. Once the raw CSI data is input into the system, pertinent pulmonary indices can be derived to estimate pulmonary function.

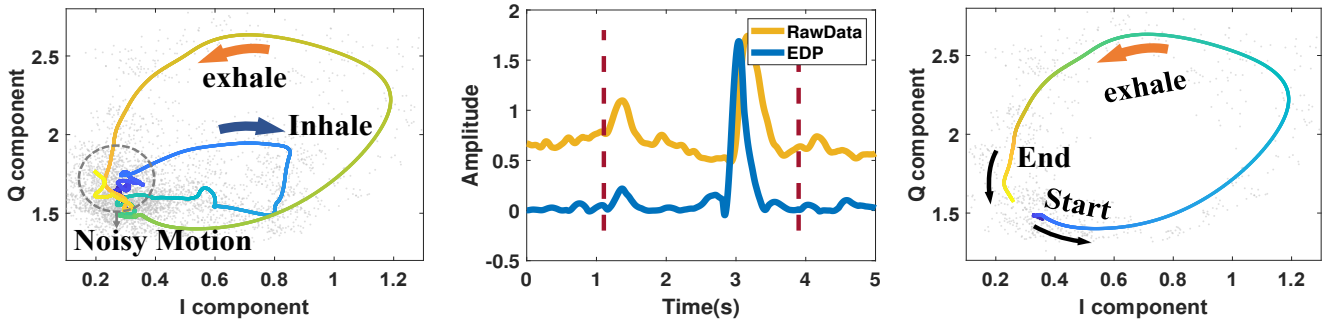

(a) CSI-ratio on the complex plane. (b) EDP of CSI-ratio. (c) Denoised exhalation

Fig. 7: Separating complete expiratory part from CSI-ratio. (a) illustrates the preliminary segmentation of a complete respiratory cycle. (b) further elucidates the refined segmentation, which pinpoints the precise commencement and conclusion of each respiration, a crucial aspect for the pulmonary function estimator. (c) isolates the denoised exhalation phase.

C. Thoracoabdominal Movement Tracker

Before feeding the CSI data into the network, we need to accurately segment the data that contains thoracoabdominal displacement movements and remove noise caused by factors such as abdominal rebound (It tends to occur at the end of exhalation) and body tremors. We first employ the Savitzky-Golay filter [41] to mitigate the influence of small-scale noisy body motions. This filter is widely recognized for its ability to preserve signal peaks, which is crucial in our case. Then, we check the variance of amplitude to roughly separate each respiration shown in Fig. 7(a). However, identifying the exact start and end moments of each respiration is still challenging due to the additional motion noise. Especially in identifying the end boundary, which is prone to be drowned out by noise for its subtle variation. Failure to accurately identify these boundaries will seriously affect the assessment of pulmonary function indices.

To tackle this problem, we utilize the Error of Dynamic Phase index (EDP-index) [26], which is proposed to quantitatively describe sensing quality, to identify the exact respiration periods. The principle of the EDP is to evaluate whether the phase variation caused by noise accounts for an excessively large proportion. As shown in Eq (1), the measured CSI phase variation is the superposition of dynamic phase variations from $\boldsymbol{H}_d$ and disturbance from ambient noise ξ. EDP assumes that higher sensing quality corresponds to a signal with less ambient noise. However, it is not feasible to directly separate the dynamic part $\boldsymbol{H}_d$ and noise ξ. By performing approximate inference operations, EDP evaluates certain statistics related to $\Delta\theta$ to measure the sensing quality of the signal. The calculation process of EDP is as follows:

$$EDP = \frac{(n-1)(\overline{\Delta\theta})^2}{\sum_{i=1}^{n}(\Delta\theta_i - \overline{\Delta\theta})^2} \tag{8}$$

where θ is the phase of the signal and $\Delta\theta$ is its corresponding variation. n is the number of samples during a time window. We calculate EDP in Fig. 7(b). Compared to the raw data, EDP allows for easier and more accurate localization of the onset

Algorithm 1 Exhalation Data Segmentation

Require: C : Filtered CSI-ratio ;
L : Sliding window size ;
Ensure: R : Fine-grained Segmentation of respiration ;
for $i \leftarrow 1$ to $\{length(C) - L\}$ **do**
  $\mu \leftarrow \frac{1}{n}\sum_{i=1}^{L} Phase(C_i)$;
  $Var = \frac{\sum_{i=1}^{L}(Phase(C_i)-\mu)^2}{L-1}$;
  if Var is peak & $Var \geq threshold_v$ **then**
    $StartTmp \leftarrow i$;
  end if
end for
$EndTmp$: The same process in loop $\{length(C)-L\} \rightarrow 1$) ;
$E \leftarrow EDP(C[startTmp : endTmp])$;
for E_i in E **do**
  if $E_i \geq threshold_E$ **then**
    $StartTmp \leftarrow i$;
  end if
end for
End : The same process in the opposite direction ;
for i in $[StartTmp : End]$ **do**
  $\overrightarrow{T_i} \leftarrow C[StartTmp + i + 1] - C[StartTmp + i]$;
  if $\overrightarrow{T_i} \times \overrightarrow{T_{i-1}} < 0$ **then**
    $Start \leftarrow i$;
  end if
end for
$R \leftarrow C[Start : End]$;
return R ;

and cessation of respiration. Then, the rotation directions of the inspiration-expiration process are calculated. As illustrated in Fig. 7(a), positive rotation directions indicate inhalation, while negative rotation directions indicate exhalation. Finally, by distinguishing the difference in rotation directions, as shown in Fig. 7(c), complete denoised exhalation data can be separated from the raw data. We further show the above process of checking the velocity of amplitude change for rough segmentation and calculating the EDP for finer segmentation in Alg. 1.

D. Pulmonary Function Estimator

*1) **Network**:* Indeed, extracting pulmonary function indices from CSI entails two steps: establishing a mapping from CSI to thoracoabdominal movements and a mapping from thoracoabdominal movements to pulmonary function indices. The complexity of the relationship between thoracoabdominal movements and lung function has been demonstrated in section II-C. It brings us considerable difficulties in recovering pulmonary function indices. The reflected signals caused by thoracoabdominal movements are superimposed, and the corresponding displacement can't be separated directly, which inevitably complicates the process of measuring pulmonary function indices. Moreover, we have to deal with the problem of insufficient generalization ability due to limited training data.

Due to the complexity of the issues mentioned, we must contemplate how to effectively extract the desired pulmonary function indices from the processed CSI data. As statistics, pulmonary function indices are deduced from the respiratory flow-time curve. Considering that the complete exhalation information is contained in the processed CSI, if we recover the respiratory flow-time curve instead of the pulmonary function indices directly with the generative model, the inherent patterns of the data may be fully explored. Inspired by the idea of variational inference (VI) [28]–[30], we aim to utilize a Variational Encoder-Decoder (VED) network equipped with excellent generalization and representation ability to solve the above problems.

The main part of our structure is an encoder $q(z|x, \theta_E)$ and a decoder $p(z|x, \theta_D)$. The encoder maps the input x to latent representation z, and then, z is fed into the decoder to generate the output (respiratory flow-time curve). Encoder parameter θ_E and decoder parameter θ_D are learned to optimize the model. The optimization process of the structure is based on VI. VI assumes that the posterior distribution is approximated by a variation distribution $q(z|x, \theta_E)$ and constructs the following optimization problem:

$$\min_{\theta} = \mathcal{D}_{KL}(q(z|x_i, \theta_E)||p(z|x_i, \theta_D)) \tag{9}$$

where $\mathcal{D}_{KL}$ is the KL divergence. Directly optimizing Eq 9 is quite challenging for the uncertainty of the true posterior distribution $p(z|x, \theta_D)$. VI adeptly reformulates this challenge as an optimization problem that involves the Evidence Lower Bound (ELBO) [28].

$$\begin{aligned}
&\log p(x_i, \theta_D) \geq ELBO \\
&= \mathbb{E}_{q(z|x,\theta_E)}[-q(z|x, \theta_E) + p(z|x, \theta_D)] \\
&= -D_{KL}(q(z|x_i, \theta_E)||p(z, \theta)) + \mathbb{E}_{q(z|x_i,\theta_E)}[\log p(x_i|z, \theta)]
\end{aligned} \tag{10}$$

where $ELBO$ is the low bound that needs to be optimized. By maximizing the $ELBO$, the VED network learns a structured and continuous latent space that establishes the connection between CSI and pulmonary function indices. This approach simplifies the cumbersome process of mapping from CSI to thoracoabdominal motion and then mapping from corresponding thoracoabdominal motion to lung function. In this way, the goal of extracting a complete respiratory flow-time curve from the CSI is achieved. The network architecture is shown in Fig. 8.

To cope with different application scenarios, we design two different training strategies as follows.

- **Personalized training:** When the patient's training sample is sufficient, and he or she can obtain accurate measurements from the medical spirometer as a label, *Wi-Pulmo* takes only labeled data from individual subjects as input to the network and produces personalized training results.
- **Group training:** When the patient's training sample is insufficient, or they cannot obtain accurate results from the medical spirometer, *Wi-Pulmo* divides the data into groups based on human factors, e.g., gender and age. This

This article has been accepted for publication in IEEE Internet of Things Journal. This is the author's version which has not been fully edited and content may change prior to final publication. Citation information: DOI 10.1109/JIOT.2024.3470321

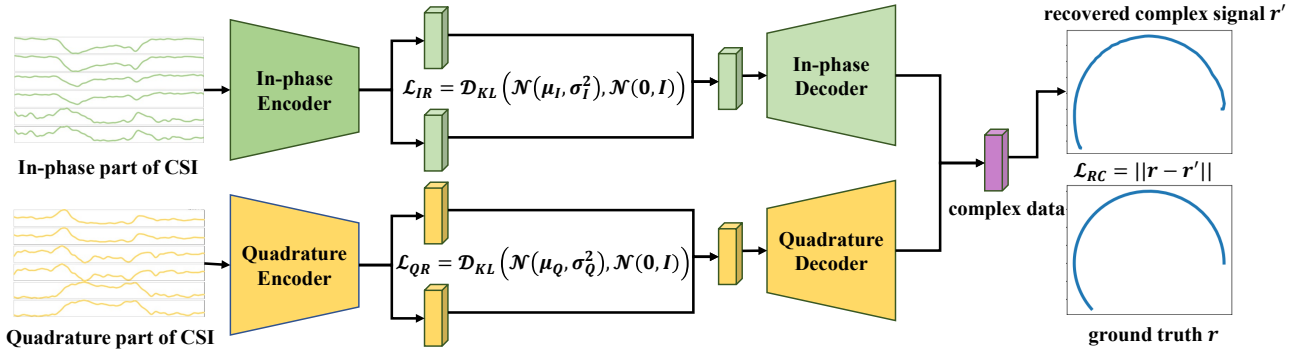

Fig. 8: Network architecture.

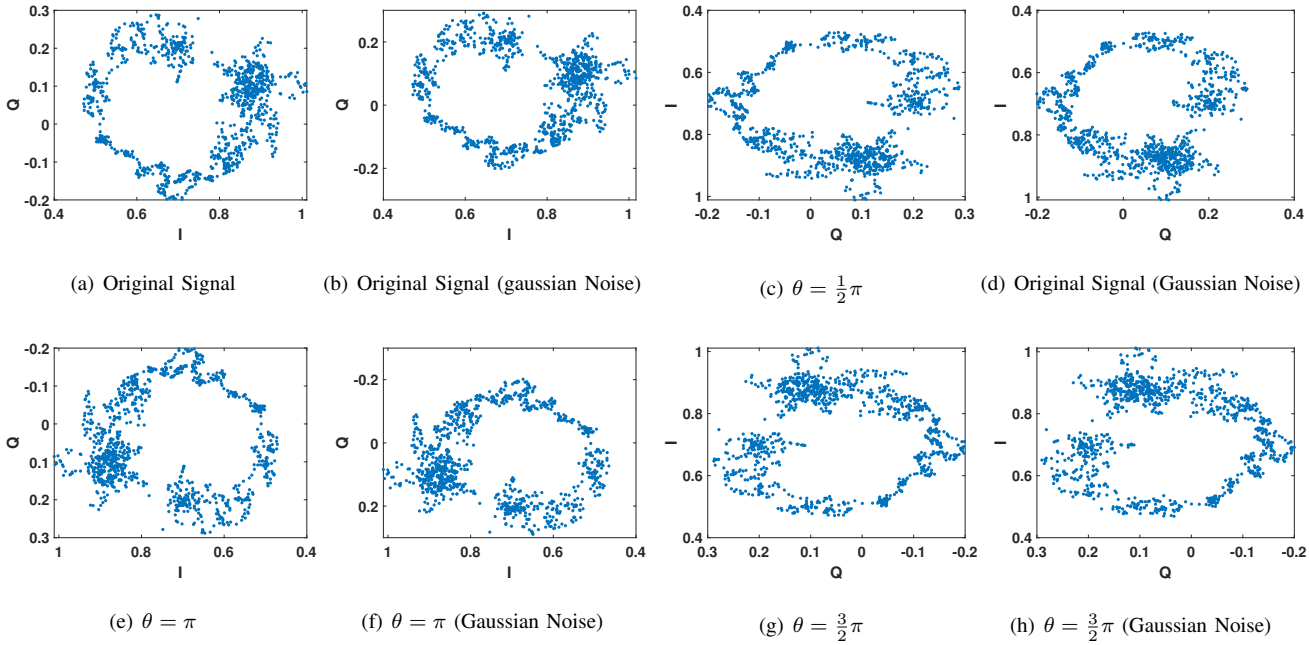

(a) Original Signal (b) Original Signal (gaussian Noise) (c) $\theta = \frac{1}{2}\pi$ (d) Original Signal (Gaussian Noise)

(e) $\theta = \pi$ (f) $\theta = \pi$ (Gaussian Noise) (g) $\theta = \frac{3}{2}\pi$ (h) $\theta = \frac{3}{2}\pi$ (Gaussian Noise)

Fig. 9: Augmenting data by rotating CSI with different angles and adding Gaussian noise.

allows them to share training data with the same group of patients.

*2) **Data augmentation**:* Firstly, we need to perform data augmentation to cope with the insufficient amount of data. Collecting a large amount of data for spirometry is challenging due to the relatively high requirements imposed on volunteers, which inevitably limits the available dataset. Data augmentation not only increases the quantity of data but also prevents the network from learning irrelevant features, which can finally improve the overall performance. Since CSI data consists of two parts, i.e., an In-phase part, and a Quadrature part, we thus can process it like images. This I/Q-induced intrinsic structure can only be preserved by rotation but not by other transforms such as translation. Therefore, as shown in Fig. 9, we rotate the data with four different angles and add Gaussian noise to them to further enhance the robustness. While our primary focus is on the change of the phase, this operation will also make our network more generalizable.

*3) **Preprocessing**:* Before feeding the data into the network, we have to address the final challenge. Spirometry data differs even when collected from the same person in the same time period. This leads to inconsistent or vastly different lengths of the CSI data after segmentation, which cannot be directly fed into the network. Although length is an important metric for measuring pulmonary function indices, arbitrary padding may introduce new noise to the CSI data. Cropping can also affect the network's accuracy. We observe that although spirometry data differ from each other, the lengths between them and their corresponding ground truth are mostly consistent. We can treat them as data pairs for resampling. If we resample each data pair with a different scale, the spirometry data themselves and the relationships between spirometry data and their ground truth still remain unchanged. Similarly, we perform the same operation on the ground truth. The specific process can be observed in the Alg. 2.

*4) **Encoder**:* When networks that are designed for complex numbers, e.g., networks in [42], [43], they have to require redefining calculus operations, e.g., differentiation, which is crucial for backpropagation. However, this operation inevitably imposes a heavy burden on training. To cope with this issue,

the encoder of our network adopts a two-stream design that is composed of the In-phase and Quadrature parts of the CSI data. This approach effectively reduces training complexity without sacrificing accuracy. We choose fine-grained segments of the CSI data as our network's input. As shown in Fig. 8, each encoder consists of a one-dimensional convolutional neural network for feature extraction. Our input is a six-channel one-dimensional sequence, and each channel is the CSI ratio [27] calculated from the three antennas relative to each other. This operation avoids selecting the so-called best CSI ratio and allows the network to take full advantage of the available data. In-phase and Quadrature parts are separated from the CSI as the final two-stream input.

The VED regularizes the latent distribution of both I/Q parts according to a standard Gaussian prior. By forcing the output of the encoder to be close to a normal distribution, VED creates structured representations in the latent space. This approach enhances VED's representation ability and helps avoid overfitting [44]. The loss calculated for regularizing I/Q parts is as follows:

$$\mathcal{L}_{IR} = \mathcal{D}_{KL}(\mathcal{N}(\mu_I, \sigma_I^2), \mathcal{N}(0, I)) \tag{11}$$

$$\mathcal{L}_{QR} = \mathcal{D}_{KL}(\mathcal{N}(\mu_Q, \sigma_Q^2), \mathcal{N}(0, I)) \tag{12}$$

where $\mathcal{D}_{KL}$ represents the calculation of KL divergence. The outputs of encoder follows the Gaussian distribution $\mathcal{N}(\mu_I, \sigma_I^2)$ and $\mathcal{N}(\mu_Q, \sigma_Q^2)$.

*5) **Decoder and Recovery Loss**:* The decoder can be considered as the reverse process of the encoder. Its goal is to recover the respiratory flow-time curve from the partial features extracted by the encoder. After obtaining the ideal complex plane data, we must measure the difference between them and the real respiratory flow-time curve. The amplitude variations in the final respiratory flow-time curve correspond to the phase changes in the output data. While the calculation of phase changes involves computing the tangential changes along the arc. It may cause trouble in backpropagation due to vector dot multiplication and division. Therefore, considering the reverse situation, we compute the mappings on the complex plane from the ground truth. The calculation results are the ground truth we want to feed into the network to measure its performance.

As shown in Alg. 2, the sampling rate of the ground truth without noise is much lower than the respiratory data. We choose to fit adjacent sample points with a linear function to increase its sampling rate up to 1kHz. Then, we resample the ground truth with the scaling ratio obtained from the previous step. Finally, we map the data onto the complex plane to generate the ground truth that is fed into the network. To make the output and ground truth similar, we employ L_2 loss to define the reconstruction loss $\mathcal{L}_{RC}$, which measures the sum of all the squared differences between them.

$$\mathcal{L}_{RC} = ||r - r'|| \tag{13}$$

Combining all these loss functions, we can obtain the total loss function as follows:

$$\mathcal{L} = \lambda(\mathcal{L}_{IR} + \mathcal{L}_{QR}) + \mathcal{L}_{RC} \tag{14}$$

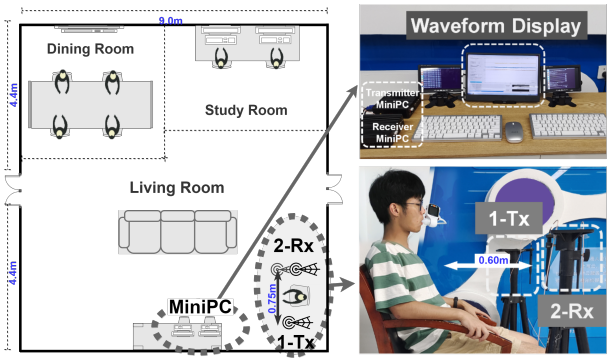

Fig. 10: Evaluation setup in the laboratory.

where λ is the weight of loss $\mathcal{L}_{IR} + \mathcal{L}_{QR}$. Since the In-phase and Quadrature parts of CSI data are equally important, they share the same weight. Moreover, based on empirical experience, we set λ to 0.1.

Algorithm 2 Ground Truth Generation

Require: S : respiratory flow-time curve of exhalation from the spirometers ;
T : Time points of curve samples ;
Z : zoom of the curve ;
Ensure: G_{cos}, G_{sin} : Ground Truth for training ;
$count \leftarrow 0$;
for s in S; t in T **do**
  $slope_i \leftarrow \frac{s_{i+1}-s_i}{t_{i+1}-t_i}$;
end for
for j in $(t_{i+1} - t_i)/[1:1000]$ **do**
  $G_{count} \leftarrow s_i + j * slope_i$;
end for
$G \leftarrow$ choose one every zoom points in G ;
$G_{cos} \leftarrow \cos(G); G_{sin} \leftarrow \sin(G)$;
return G_{cos}, G_{sin} ;

*6) **Respiratory Flow-Time Curve recovery**:* Considering the challenges discussed in the preceding section, we opt to map the amplitude fluctuations of the original respiratory flow-time curve to the phase variations of the circular arc in the complex plane. The proposed network exclusively generates the exhalation component. Following the completion of network training, we can retrieve the respiratory flow-time curve by applying the reverse process outlined in Alg. 2. Similarly, other pulmonary function indices can be directly calculated, which is the same process as the spirometer.

IV. Evaluation in Laboratory

A. Evaluation Setup

As illustrated in Fig. 10, *Wi-Pulmo* establishes an experimental room in a home-like environment with dimensions of $10.4 \times 9.0m^2$. The setup includes a sofa placed in the center, while other furniture items are positioned along the walls to simulate a living room atmosphere. Adjacent to the living room is a dining room and a study room, which are separated by glass doors. *Wi-Pulmo* is installed in the lower right corner of the living room. This experimental

This article has been accepted for publication in IEEE Internet of Things Journal. This is the author's version which has not been fully edited and content may change prior to final publication. Citation information: DOI 10.1109/JIOT.2024.3470321

TABLE I: Subject demographics.

Category	Characteristics	Number
Demo-graphics	Patient Num.	10
	Test per person	39.2±4.6
	Female(%)	5 (50%)
Body conditions	Age (years)	22.9±1.4
	Height(cm)	170.1±7.1
	Weight(kg)	58.9±9.1
	Body Mass Index (BMI) (kg/m^2)	20.3±2.5
	Normal (%)	8 (80%)
	Underweight (%)	2 (20%)

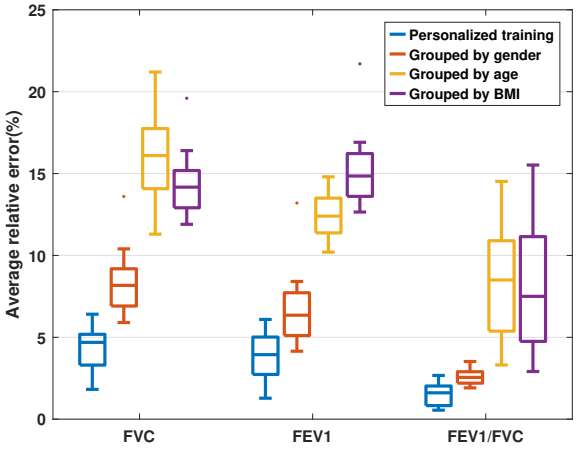

Fig. 11: Overall accuracy of *Wi-Pulmo* with different training strategies.

arrangement allows us to assess the robustness of *Wi-Pulmo* in real-life scenarios comprehensively. The bottom part of the figure displays our experimental equipment, which mainly consists of two MiniPCs featuring a 2.16GHz CPU, 4GB RAM, and 240GB SSD. These MiniPCs are equipped with Intel 5300 network interface cards and employ the CSITOOL [45] software for the transmission and collection of CSI data. The distance between the two transceivers is fixed at 0.75m, and the subject is positioned at a distance of 0.6m from the transceivers.

We recruit a total of 10 healthy young subjects, including 5 females and 5 males, to participate in our experiments conducted in a laboratory environment. The demographic data and physiological condition statistics of the participants are presented in Tab. I. Apart from a few individuals who are either overweight or underweight, which could potentially influence the test results, all other participants exhibited normal values for various physical indices.

Furthermore, we acquire a medical spirometer (model SP-70B) to measure real respiratory flow-time curves, which served as a reference for our study (ground truth). Each volunteer is instructed to adhere to the pulmonary volume measurement method outlined in Sec. II to complete the experiments. Specifically, volunteers are seated upright on a chair with a slight backward tilt, which ensures their backs are firmly against the chair. They are directed to hold the handles with both hands, which allows their chests to be exposed and maintains a relaxed posture as much as possible. The spirometer is securely positioned using a stand, which enables volunteers to focus solely on exhaling during each trial. This testing approach enhances the efficiency of our experiments while ensuring accurate and reliable results.

Ultimately, we collect an average of 39.2 ± 4.6 sets of data from each volunteer for personalized training with *Wi-Pulmo*, which is considered sufficient for individual users. However, not all participants are able to undergo direct data collection using the spirometer. Instead, they have to rely on training results obtained from other individuals. This approach is necessary for the implementation of both personalized training strategies and group training strategies.

B. Overall Accuracy

As mentioned in the earlier analysis, when deploying *Wi-Pulmo* for practical use, we encounter challenges such as insufficient individual samples or a lack of ground truth for comparison. To address these issues, we design two targeted training strategies in Sec. III-D.

As illustrated in Fig. 11, among both of the training strategies, the personalized training method undoubtedly yielded the best results, with error rates of $4.21\%\pm1.42\%$, $3.78\%\pm1.53\%$, and $1.50\% \pm 0.69\%$ for FVC, FEV1, and FEV1/FVC indexes, respectively. In contrast, the group training method exhibits inferior performance compared to the personalized training method due to the diverse characteristics of individuals within a group, which demonstrates the necessity of the reliance on grouping strategies. When grouped by gender, *Wi-Pulmo* achieves the minimum error rates of $8.32\% \pm 2.07\%$, $6.86\% \pm 2.34\%$, and $2.59\% \pm 0.49\%$ for FVC, FEV1, and FEV1/FVC indices, respectively. This result is consistent with the conclusion that pulmonary function varies significantly between males and females due to inherent differences in body structure [46]. Hence, we select gender as the only group factor in the following content, and the principle is also followed in the clinic study. Compared to the clinical spirometers, which usually yield a result within 3% error [15], *Wi-Pulmo* demonstrates a comparable level of accuracy to in-clinic spirometry, which further affirms its suitability for clinical investigations.

C. Effectiveness of Noise Removal

During practical testing, *Wi-Pulmo* inevitably encounters noise caused by body tremors at the start and end of respiration, which significantly affects the data's validity. This issue becomes particularly challenging when conducting tests in a hospital environment, where it is difficult to expect elderly patients to maintain a relaxed and stable posture during PFT. We need to remove this noise by exactly locating the onset and cessation of respiration. Therefore, the implementation of

This article has been accepted for publication in IEEE Internet of Things Journal. This is the author's version which has not been fully edited and content may change prior to final publication. Citation information: DOI 10.1109/JIOT.2024.3470321

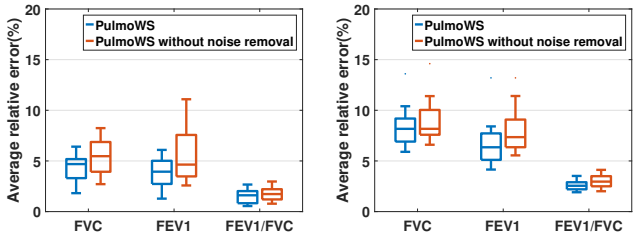

(a) Personalized training. (b) Group training.

Fig. 12: Effectiveness of noise removal.

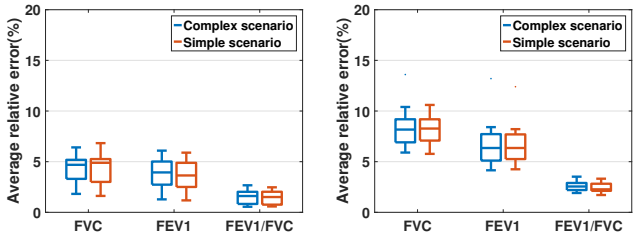

(a) Personalized training. (b) Group training.

Fig. 13: Impact of different scenarios.

our thoracoabdominal movement tracker is crucial, and we investigate the effectiveness of noise removal in both training strategies in this section. As illustrated in Fig. 12, without the support from Alg. 1, an increase in error rates for all three PFT indices is found regardless of the training strategy. In particular, the error rate of FEV1 varies the most, ranging from $3.78\% \pm 1.53$ to $5.63\% \pm 2.78$ in personalized training and from $6.86\% \pm 2.34$ to $8.04\% \pm 2.26$ in group training. The decline not only highlights the significant impact of noise from body tremors on the results but also confirms the effectiveness of our noise removal module.

D. Impact of Different Scenarios

The performance of WiFi sensing is easily affected by environmental noise and multipath reflections. As shown in Fig. 10, a home-like environment with many pieces of furniture and electrical appliances creates rich multipath reflections, which may seriously interfere with our sensing quality.

In this section, we evaluate our system in a completely new scenario for comparison. We maintain the placement of our experimental equipment unchanged and remove bulky items such as the sofa. This allows us to create an empty experimental scenario where our CSI data is barely impacted by other clutter except for our experimenter. However, the impact of noise caused by human body motion will be amplified in this scenario. This situation places high demands on the robustness of our system.

Fig. 13 illustrates the comparison results between the two scenario experiments. Overall, the results of the two experiments are almost identical, which clearly suggests that surrounding clutter has a limited impact on our system, whether in a complex furnished scenario or an empty scenario. Due to the strong generalization ability of the network, the out-of-training data are hardly affected by simple environmental changes. This proves that *Wi-Pulmo* has strong robustness to environmental changes.

TABLE II: Correlation between lung function indices and Human Factors (Laboratory).

Corr. Coeff. (P-value)	FVC	FEV1	FEV1/FVC
Gender	0.90 (0.008)	0.83 (0.006)	0.31 (0.31)
Age	0.31 (0.41)	0.35 (0.35)	0.16 (0.16)
Body Mass Index (BMI)	0.70 (0.04)	0.70 (0.04)	0.09 (0.81)

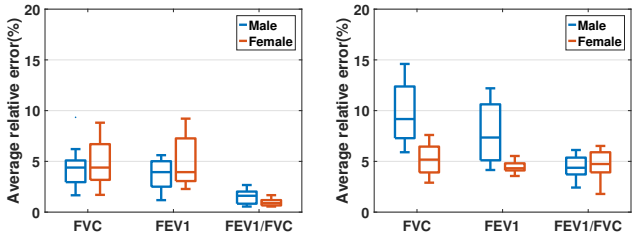

(a) Personalized training. (b) Group training.

Fig. 14: Impact of gender.

E. Impact of Human Factors on Wi-Pulmo

We will conduct an analysis using Pearson correlation coefficients to examine the relationship between human factors and pulmonary function indices in this section. This analysis aims to elucidate the rationale behind the proposed grouping strategy. The results presented in Tab. II demonstrate a significant correlation between gender and BMI with pulmonary function indices. For instance, gender exhibits the strongest association with the FVC index($P < 0.01$). While it is widely acknowledged that age is a crucial factor that influences pulmonary function indices, our observations in the laboratory testing environment, where participants have similar ages, do not reveal a substantial correlation between age and pulmonary function indices. Nevertheless, our experiments conducted in a hospital environment confirm the anticipated correlation between age and pulmonary function indices. To better evaluate the *Wi-Pulmo* robustness, we primarily focus on the three features highlighted in Tab. II.

Gender: As illustrated in Fig. 14, the two employed training strategies produce contrasting outcomes when considering gender as a factor. In personalized training, males exhibit lower errors and greater stability in both FVC and FEV1. However, the opposite trend is observed in group training. This disparity could be attributed to inherent disparities in physical fitness between males and females, with males naturally possessing stronger pulmonary function [46]. We hypothesize that during the testing process, the variations in chest wall movement are more pronounced in males compared to females, and the differences in body composition between genders magnify this

This article has been accepted for publication in IEEE Internet of Things Journal. This is the author's version which has not been fully edited and content may change prior to final publication. Citation information: DOI 10.1109/JIOT.2024.3470321

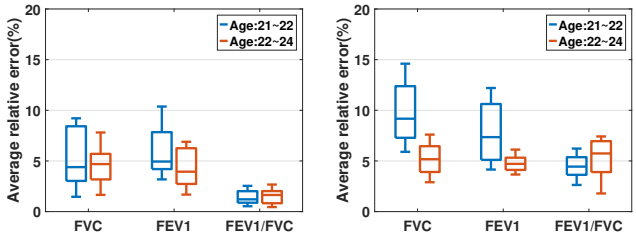

(a) Personalized training. (b) Group training.

Fig. 15: Impact of age.

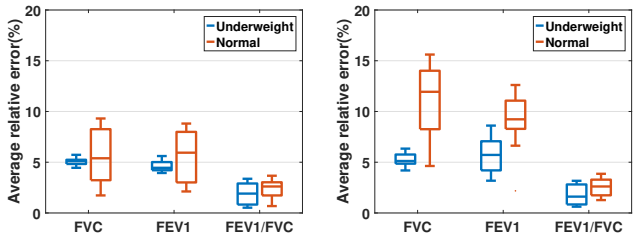

(a) Personalized training. (b) Group training.

Fig. 16: Impact of BMI.

distinction. Consequently, the changes in males are more easily detected by the WiFi, which results in more accurate results.

Age: As shown in Fig. 15, we categorize the test subjects into two age groups, i.e., 21 to 22 years and 23 to 24 years. It is observed that irrespective of the training strategy, *Wi-Pulmo* exhibits superior performance in the older age group. Research indicates that human pulmonary function reaches its peak between the ages of 20 and 25 [47]. The chosen participants conveniently fall within this age range. Furthermore, within this specific age range, pulmonary function tends to stabilize as individuals grow older.

BMI: The impact of body composition on pulmonary function indices is evident. Research has demonstrated that underweight individuals exhibit reduced pulmonary function indices, especially for FVC and FEV1. Body composition encompasses various factors, such as height, weight, and body fat percentage. In our study, we employ BMI as a simplified criterion to classify individuals into two groups, i.e., subjects with low or normal BMI. Fig. 16 shows the impact of BMI on recognition performance. We can observe that *Wi-Pulmo* has better recognition performance for individuals with lower BMI, which can be attributed to their ability to achieve a more relaxed state during PFT and minimize noise disturbances caused by body tremors.

V. Clinic Study

Experiments are successfully conducted within our laboratory environment. To assess the robustness of our system, further experiments are performed in a hospital setting. A 2-month clinical study is conducted at a city hospital in accordance with the guidelines of EC approval.

A. Clinical Evaluation Setup

Wi-Pulmo, as depicted in Fig. 17, requires patients to undergo the same pulmonary function test process as conducted

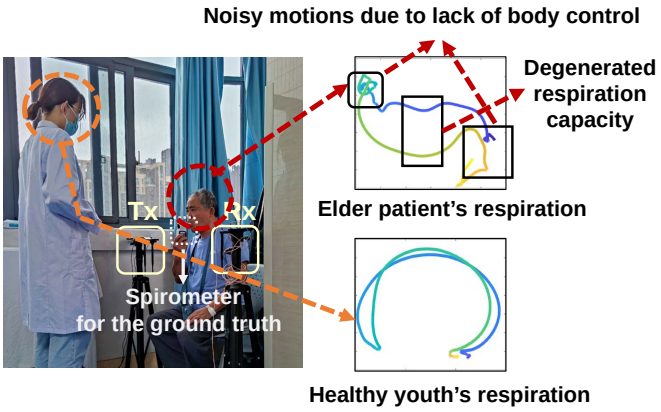

Fig. 17: Setup in the clinical study.

TABLE III: Subject demographics.

Category	Characteristics	Number
Demo-graphics	Patient Num.	34
	Test per person	7.1± 1.6
	Validate Test per person	3.6± 1.5
	Female(%)	12 (35.2%)
Body Conditions	Age (years)	66.7 ± 15.6
	Height(cm)	166.4 ± 7.7
	Weight(kg)	69.1 ± 16.1
	BMI(kg/m^2)	24.9 ± 5.2
Diseases	Coronary Heart Disease(%)	64.7 %
	High Blood Pressure (%)	58.8 %
	Brain Infarction (%)	29.4 %
	Heart Failure (%)	17.6 %

in the laboratory. While this procedure may be straightforward for young and healthy individuals, elderly patients often face challenges in adhering to the standardized spirometry protocol. Among the 52 hospitalized patients recruited for the study, only 34 of them are able to successfully complete at least one accurate pulmonary function test. The natural decline in cognitive abilities among elderly individuals necessitates additional time and effort for them to familiarize themselves with the procedure. Moreover, many patients struggle to manage their body adjustments during the test maneuvers. Individuals with compromised pulmonary function find it particularly difficult to generate the necessary depth of breath required for accurate test results.

Tab. III presents the information of these 34 patients. This phenomenon is consistent with our statistics, which indicate that female cardiovascular patients account for a lower percentage (35.2%), as supported by previous research [48]. Therefore, gender remains one of the primary factors that we need to focus on. The major distinction between the hospital and laboratory environments lies in the fact that the individuals tested in the hospital setting mostly have underlying medical conditions. Notably, as shown in Tab. III, coronary heart disease consists of 64.7% of the participants in our study.

This article has been accepted for publication in IEEE Internet of Things Journal. This is the author's version which has not been fully edited and content may change prior to final publication. Citation information: DOI 10.1109/JIOT.2024.3470321

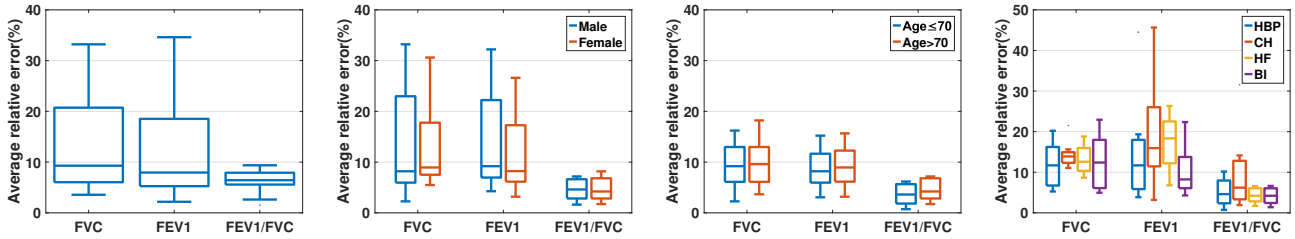

(a) Average errors of pulmonary function indices (b) Impact of gender (c) Impact of age (d) Impact of disease

Fig. 18: Performance evaluation in the clinical study.

TABLE IV: Correlation between lung function indices and Human Factors (clinical).

Corr. Coeff. (P-value)	**FVC**	**FEV1**	**FEV1/FVC**
Gender	0.53 (0.02)	0.58 (0.01)	0.25 (0.32)
Age	0.42 (0.09)	0.46 (0.06)	0.06 (0.82)
High Blood Pressure (HBP)	0.009 (0.97)	0.08 (0.75)	0.34 (0.17)
Coronary Heart (CH)	0.09 (0.72)	0.13 (0.60)	0.25 (0.32)
Heart Failure (HF)	0.33 (0.20)	0.35 (0.17)	0.09 (0.70)
Brain Infarction (BI)	0.08 (0.75)	0.09 (0.73)	0.003 (0.99)

B. Correlation between Pulmonary Function and Human Factors

We present a summary of the Pearson correlation between pulmonary function indices and human factors, including gender, age, and diseases, in Tab. IV. The diseases are further categorized into four groups as described in Tab. III. On average, each patient experiences 2.6 underlying diseases. Older adults exhibit a decline in pulmonary function compared to younger individuals, with the decline becoming more pronounced with increasing age. This observation highlights the importance of age as a critical factor influencing pulmonary function. Previous research [49] has demonstrated the significant impact of chronic diseases such as high blood pressure (HBP) on pulmonary function. The widespread adoption of daily pulmonary function testing not only benefits patients with pulmonary conditions such as COPD but also offers significant advantages to the 1.13 billion individuals globally affected by hypertension. Besides, gender remains the most influential factor in pulmonary function.

C. Performance Evaluation

Due to the physical condition of elderly individuals, the majority of them are unable to undergo extensive experimentation like younger individuals in a laboratory environment. On average, we collect only 7.1 sets of data per subject. After excluding the unusable data resulting from non-compliant procedures, we are left with only 3.6 sets for each subject. This presents a significant challenge for our analysis, which renders the previously used personalized training approach ineffective due to the limited sample size. Therefore, our subsequent analysis is based on group training. Due to the previous discussion on the differences in lung function between males and females, we still consider gender factor as the only criterion determining the grouping.

The overall error obtained from our experiments conducted in the hospital is shown in Fig. 18(a). The FVC, FEV1, and FEV1/FVC indices achieve error rates of $13.59\% \pm 10.05\%$, $11.56\% \pm 9.43\%$, and $5.87\% \pm 2.29\%$, respectively. Compared to the performance of younger individuals, the error rates of all indices increase significantly. As mentioned in the previous section, standard PFT is a rigorous and physically demanding activity. We observe that in actual practice, it is quite difficult for most elderly people to complete such a challenging task. Additionally, the health status of the elderly is generally worse than that of younger individuals, leading to greater variability in their pulmonary function. These phenomena explain why our system performs worse on the elderly. We further analyze the following three relevant factors:

Gender: As shown in Fig. 18(b), we obtained similar results as before, with slightly higher errors in males compared to females. This suggests that even among older people, inherent disparities in physical fitness between males and females persist. Also, due to worse health, the overall errors are slightly larger compared to the measurements conducted in the laboratory.

Age: Fig. 18(c) divides the patients into two age groups (age ≤ 70 and age > 70), and the older age group exhibited slightly higher errors in their data. This finding is consistent with our understanding of their physical condition and the fact that pulmonary function decreases with age.

Disease: In Fig. 18(d), we observe significant differences in the values of Coronary Heart (CH) compared to other diseases in the disease grouping. It shows good performance in FVC, but the errors are larger in FEV1 and FEV1/FVC. This is because cardiovascular diseases can reduce the patient's ability to absorb oxygen in the bloodstream, which leads to increased respiratory rate and faster completion of non-standard PFT. Patients may exhibit larger motion amplitudes during the measurement process, which inevitably results in increased errors for FEV1. No significant abnormalities are

observed in the data for the other diseases.

This result shows a significant discrepancy compared to the results obtained from our laboratory data collection. The data errors for some individual patients are even unacceptably high. Through our analysis, we attribute this difference to the greater level of uncontrollable factors associated with data collection from elderly patients. As mentioned in the previous paragraph, even half of the data collected from elderly patients is unusable. Additionally, the diverse range of human factors inherent in these elderly patients may necessitate conducting experiments over a longer period. Overall, the experiments conducted in the hospital have provided evidence for the clinical value of *Wi-Pulmo*. The results are consistent with our expectations. However, it is important to note that the testing process in the actual clinical environment is more complex and requires more comprehensive consideration of multiple factors. In light of the aforementioned challenges, further research is warranted to explore strategies that can facilitate a more seamless completion of the experiments by the patients. Considering their reduced energy levels compared to younger individuals, such efforts will not only alleviate their burden but also enhance the accuracy of our findings.

VI. Conclusion

We propose *Wi-Pulmo*, an end-to-end learning-based Wireless System that utilizes WiFi CSI to provide contact-free, convenient, cost-effective, and precise Pulmonary Function Testing outside the clinical setting. The fundamental concept is to employ WiFi CSI to capture thoracoabdominal movement patterns and translate this information into pulmonary function metrics. We first carefully design an efficient algorithm to accurately segment the data that contains the respiration from the raw noisy CSI data. Then, we feed the fine-grained segment data into a novel VED network. To address the problem of insufficient data, we devise two target training algorithms. We also carefully analyze the feasibility of using CSI to measure lung function from a medical perspective. By conducting an extensive range of experiments in laboratory and clinical scenarios, we obtain encouraging and favorable outcomes. Our studies unequivocally demonstrate that *Wi-Pulmo* exhibits convenience, efficiency, high precision, and affordability. As such, it represents a reliable and practical solution for daily monitoring, which proves particularly valuable for elderly individuals with underlying medical conditions.

Acknowledgments

This work is supported by the National Natural Science Foundation of China (Grant No. 62302145, No. U23A20303, and No. 62372149), Anhui Province Science Foundation for Youths (Grant No. 2308085QF230), and the Major scientific and technological project of Anhui Provincial Science and Technology Innovation Platform (Grant No. 202305a12020012). We would like to thank the editors and anonymous reviewers for their insightful comments and constructive feedback.

References

[1] G. Wang, J. Hallberg, R. Faner, H.-J. Koefoed, S. Kebede Merid, S. Klevebro, S. Björkander, O. Gruzieva, G. Pershagen, M. van Hage, S. Guerra, M. Bottai, A. Georgelis, U. Gehring, A. Bergström, J. M. Vonk, I. Kull, G. H. Koppelman, A. Agusti, and E. Melén, "Plasticity of individual lung function states from childhood to adulthood," *American Journal of Respiratory and Critical Care Medicine*, vol. 207, no. 4, pp. 406–415, 2023, pMID: 36409973. [Online]. Available: https://doi.org/10.1164/rccm.202203-0444OC

[2] M. J. Hegewald, H. M. Gallo, and E. L. Wilson, "Accuracy and quality of spirometry in primary care offices," *Annals of the American Thoracic Society*, vol. 13, no. 12, pp. 2119–2124, 2016.

[3] S. Lutfiyah, R. E. Yuwana, and H. G. Ariswati, "Design and development of an iot-based pulmonary function and oxygen saturation measurement device," *Indonesian Journal of Electronics, Electromedical Engineering, and Medical Informatics*, vol. 6, no. 1, pp. 34–42, Feb. 2024. [Online]. Available: https://ijeeemi.poltekkesdepkes-sby.ac.id/index.php/ijeeemi/article/view/310

[4] M. Kong, J. An, D. Jung, and T. Hong, "Occupant-centered indoor environmental quality management: Physiological response measuring methods," *Building and Environment*, vol. 243, p. 110661, 2023. [Online]. Available: https://www.sciencedirect.com/science/article/pii/S0360132323006881

[5] J. Cao, Y. Wang, H. Tao, and X. Guo, "Sensor-based human activity recognition using graph lstm and multi-task classification model," *ACM Trans. Multimedia Comput. Commun. Appl.*, vol. 18, no. 3s, oct 2022. [Online]. Available: https://doi.org/10.1145/3561387

[6] D. McDuff, "Camera measurement of physiological vital signs," *ACM Comput. Surv.*, vol. 55, no. 9, jan 2023. [Online]. Available: https://doi.org/10.1145/3558518

[7] A. P. Addison, P. S. Addison, P. Smit, D. Jacquel, and U. R. Borg, "Noncontact respiratory monitoring using depth sensing cameras: A review of current literature," *Sensors*, vol. 21, no. 4, 2021. [Online]. Available: https://www.mdpi.com/1424-8220/21/4/1135

[8] M. Mozafari, A. J. Law, J. R. Green, and R. A. Goubran, "Respiration rate estimation from thermal video of masked and unmasked individuals using tensor decomposition," in *2022 IEEE International Instrumentation and Measurement Technology Conference (I2MTC)*, 2022, pp. 1–5.

[9] X. Lan, Y. Yuan, X. Wang, Z. Wang, and W. Zhu, "A survey on temporal sentence grounding in videos," *ACM Trans. Multimedia Comput. Commun. Appl.*, vol. 19, no. 2, feb 2023. [Online]. Available: https://doi.org/10.1145/3532626

[10] Z. Xie, J. Chen, K. Wu, D. Guo, and R. Hong, "Global temporal difference network for action recognition," *IEEE Transactions on Multimedia*, vol. 25, pp. 7594–7606, 2023.

[11] M. Goel, E. Saba, M. Stiber, E. Whitmire, J. Fromm, E. C. Larson, G. Borriello, and S. N. Patel, *SpiroCall: Measuring Lung Function over a Phone Call*. New York, NY, USA: Association for Computing Machinery, 2016, p. 5675–5685. [Online]. Available: https://doi.org/10.1145/2858036.2858401

[12] J. Huang, J.-X. Bai, X. Zhang, Z. Liu, Y. Feng, J. Liu, X. Sun, M. Dong, and M. Li, "Keystrokesniffer: An off-the-shelf smartphone can eavesdrop on your privacy from anywhere," *IEEE Transactions on Information Forensics and Security*, vol. 19, pp. 6840–6855, 2024.

[13] S. Bhalla, S. Liaqat, R. Wu, A. S. Gershon, E. de Lara, and A. Mariakakis, "Pulmolistener: Continuous acoustic monitoring of chronic obstructive pulmonary disease in the wild," *Proc. ACM Interact. Mob. Wearable Ubiquitous Technol.*, vol. 7, no. 3, sep 2023. [Online]. Available: https://doi.org/10.1145/3610889

[14] X. Yin, K. Huang, E. Forno, W. Chen, H. Huang, and W. Gao, "Ptease: Objective airway examination for pulmonary telemedicine using commodity smartphones," in *Proceedings of the 21st Annual International Conference on Mobile Systems, Applications and Services*, ser. MobiSys '23. New York, NY, USA: Association for Computing Machinery, 2023, p. 110–123. [Online]. Available: https://doi.org/10.1145/3581791.3596854

[15] X. Song, B. Yang, G. Yang, R. Chen, E. Forno, W. Chen, and W. Gao, "Spirosonic: monitoring human lung function via acoustic sensing on commodity smartphones," in *MobiCom '20: The 26th Annual International Conference on Mobile Computing and Networking, London, United Kingdom, September 21-25, 2020*. ACM, 2020, pp. 52:1–52:14.

[16] H. Yan, Y. Zhang, Y. Wang, and K. Xu, "Wiact: A passive wifi-based human activity recognition system," *IEEE Sensors Journal*, vol. 20, no. 1, pp. 296–305, 2019.

[17] Y. Zhang, F. Han, P. Yang, Y. Feng, Y. Yan, and R. Guan, "Wi-cyclops: Room-scale wifi sensing system for respiration detection based on single-antenna," *ACM Trans. Sen. Netw.*, vol. 20, no. 4, may 2024. [Online]. Available: https://doi.org/10.1145/3632958

[18] D. Fan, X. Yang, N. Zhao, L. Guan, M. M. Arslan, M. Ullah, M. A. Imran, and Q. H. Abbasi, "A contactless breathing pattern recognition system using deep learning and wifi signal," *IEEE Internet of Things Journal*, pp. 1–1, 2024.

[19] X. Zhang, Y. Gu, H. Yan, Y. Wang, M. Dong, K. Ota, F. Ren, and Y. Ji, "Wital: A cots wifi devices based vital signs monitoring system using nlos sensing model," *IEEE Transactions on Human-Machine Systems*, pp. 1–13, 2023.

[20] Y. Gu, X. Zhang, Z. Liu, and F. Ren, "Wifi-based real-time breathing and heart rate monitoring during sleep," in *2019 IEEE Global Communications Conference (GLOBECOM)*. IEEE, 2019, pp. 1–6.

[21] Y. Gu, X. Zhang, H. Yan, Z. Liu, and Y. Ji, "Real-time vital signs monitoring based on cots wifi devices," in *2021 IEEE International Conference on Bioinformatics and Biomedicine (BIBM)*. IEEE, 2021, pp. 1320–1324.

[22] Y. Qiao, K. Wu, and X. Yuan, "Autotomo: Learning-based traffic estimator incorporating network tomography," *IEEE/ACM Transactions on Networking*, pp. 1–16, 2024.

[23] Y. Qiao, Y. Xinyu, and K. Wu, "Routing-oblivious network tomography with flow-based generative model (accepted)," *IEEE International Conference on Computer Communications*, 2024.

[24] M. Setiawan, M. A. Malik, and K. Fobelets, "Correlation between smart mask and knitted coil sensors breathing data," *Engineering Proceedings*, vol. 52, no. 1, 2023. [Online]. Available: https://www.mdpi.com/2673-4591/52/1/15

[25] A. Houssein, D. Ge, S. Gastinger, R. Dumond, and J. Prioux, "Estimation of respiratory variables from thoracoabdominal breathing distance: a review of different techniques and calibration methods," *Physiological measurement*, vol. 40, no. 3, p. 03TR01, 2019.

[26] R. Gao, W. Li, Y. Xie, E. Yi, L. Wang, D. Wu, and D. Zhang, "Towards robust gesture recognition by characterizing the sensing quality of wifi signals," *Proceedings of the ACM on Interactive, Mobile, Wearable and Ubiquitous Technologies*, vol. 6, pp. 1–26, 03 2022.

[27] Y. Zeng, D. Wu, J. Xiong, E. Yi, R. Gao, and D. Zhang, "Farsense: Pushing the range limit of wifi-based respiration sensing with csi ratio of two antennas," *Proceedings of the ACM on Interactive, Mobile, Wearable and Ubiquitous Technologies*, vol. 3, no. 3, pp. 1–26, 2019.

[28] D. Blei, A. Kucukelbir, and J. McAuliffe, "Variational inference: A review for statisticians," *Journal of the American Statistical Association*, vol. 112, 01 2016.

[29] D. P. Kingma and M. Welling, "Auto-encoding variational bayes," 2013. [Online]. Available: https://arxiv.org/abs/1312.6114

[30] T. Zheng, Z. Chen, S. Zhang, C. Chao, and J. Luo, "More-fi: Motion-robust and fine-grained respiration monitoring via deep-learning uwb radar," 11 2021.

[31] O. N. Obi, S. Alqalyoobi, V. Maddipati, E. E. Lower, and R. P. Baughman, "High-resolution ct scan fibrotic patterns in stage iv pulmonary sarcoidosis: Impact on pulmonary function and survival," *CHEST*, vol. 165, no. 4, pp. 892–907, 2024. [Online]. Available: https://www.sciencedirect.com/science/article/pii/S0012369223056660

[32] H. Zhao, Y. Zhang, X. Huang, and Y. Xiang, "An adaptive physical layer key extraction scheme for smart homes," in *2019 18th IEEE International Conference On Trust, Security And Privacy In Computing And Communications/13th IEEE International Conference On Big Data Science And Engineering (TrustCom/BigDataSE)*, 2019, pp. 499–506.

[33] J. Huang, B. Liu, C. Miao, X. Zhang, J. Liu, L. Su, Z. Liu, and Y. Gu, "Phyfinatt: An undetectable attack framework against phy layer fingerprint-based wifi authentication," *IEEE Transactions on Mobile Computing*, vol. 23, no. 7, pp. 7753–7770, 2024.

[34] P. Yu, J. Zhang, H. Fang, W. Li, L. Feng, F. Zhou, P. Xiao, and S. Guo, "Digital twin driven service self-healing with graph neural networks in 6g edge networks," *IEEE Journal on Selected Areas in Communications*, vol. 41, no. 11, pp. 3607–3623, 2023.

[35] D. Zhang, K. Niu, J. Xiong, F. Zhang, and X. Wang, *WiFi/4G/5G Based Wireless Sensing: Theories, Applications and Future Directions*. Singapore: Springer Nature Singapore, 2023, pp. 387–417. [Online]. Available: https://doi.org/10.1007/978-981-99-2501-8_14

[36] J. Huang, B. Liu, C. Miao, Y. Lu, Q. Zheng, Y. Wu, J. Liu, L. Su, and C. W. Chen, "Phaseanti: An anti-interference wifi-based activity recognition system using interference-independent phase component," *IEEE Transactions on Mobile Computing*, vol. 22, no. 5, pp. 2938–2954, 2023.

[37] P. Yu, Y. Ding, Z. Li, J. Tian, J. Zhang, Y. Liu, W. Li, and X. Qiu, "Energy-efficient coverage and capacity enhancement with intelligent uav-bss deployment in 6g edge networks," *IEEE Transactions on Intelligent Transportation Systems*, vol. 24, no. 7, pp. 7664–7675, 2023.

[38] M. Ba, P. Pianosi, and R. Rajamani, "Estimation of respiratory displacements using a nonlinear observer," *IFAC-PapersOnLine*, vol. 56, no. 3, pp. 283–288, 2023, 3rd Modeling, Estimation and Control Conference MECC 2023. [Online]. Available: https://www.sciencedirect.com/science/article/pii/S2405896323023716

[39] G. Johnson, P. Pianosi, and R. Rajamani, "Estimation of three-dimensional thoracoabdominal displacements during respiration using inertial measurement units," *IEEE/ASME Transactions on Mechatronics*, vol. 27, no. 6, pp. 4224–4234, 2022.

[40] B. Sheng, R. Han, F. Xiao, Z. Guo, and L. Gui, "Metaformer: Domain-adaptive wifi sensing with only one labelled target sample," *Proc. ACM Interact. Mob. Wearable Ubiquitous Technol.*, vol. 8, no. 1, mar 2024. [Online]. Available: https://doi.org/10.1145/3643550

[41] J. Dai, E. Jamalinia, N. R. Vaughn, R. E. Martin, M. König, K. L. Hondula, J. Calhoun, J. Heckler, and G. P. Asner, "A general methodology for the quantification of crop canopy nitrogen across diverse species using airborne imaging spectroscopy," *Remote Sensing of Environment*, vol. 298, p. 113836, 2023. [Online]. Available: https://www.sciencedirect.com/science/article/pii/S0034425723003875

[42] T. E. Potok, C. Schuman, S. Young, R. Patton, F. Spedalieri, J. Liu, K.-T. Yao, G. Rose, and G. Chakma, "A study of complex deep learning networks on high-performance, neuromorphic, and quantum computers," vol. 14, no. 2, 2018. [Online]. Available: https://doi.org/10.1145/3178454

[43] C. Trabelsi, O. Bilaniuk, Y. Zhang, D. Serdyuk, S. Subramanian, J. F. Santos, S. Mehri, N. Rostamzadeh, Y. Bengio, and C. J. Pal, "Deep complex networks," 2017. [Online]. Available: https://arxiv.org/abs/1705.09792

[44] J. Liu, S. Wang, H. Xu, Y. Xu, Y. Liao, J. Huang, and H. Huang, "Federated learning with experience-driven model migration in heterogeneous edge networks," *IEEE/ACM Transactions on Networking*, pp. 1–17, 2024.

[45] D. Halperin, W. Hu, A. Sheth, and D. Wetherall, "Tool release: Gathering 802.11n traces with channel state information," *ACM SIGCOMM CCR*, vol. 41, no. 1, p. 53, Jan. 2011.

[46] W. M. Vollmer, P. L. Enright, K. L. Pedula, F. Speizer, L. H. Kuller, J. Kiley, and G. G. Weinmann, "Race and gender differences in the effects of smoking on lung function," *Chest*, vol. 117, no. 3, pp. 764–772, 2000.

[47] A. E. Marossy, D. P. Strachan, A. R. Rudnicka, and H. R. Anderson, "Childhood chest illness and the rate of decline of adult lung function between ages 35 and 45 years," *American journal of respiratory and critical care medicine*, vol. 175, no. 4, pp. 355–359, 2007.

[48] Z. Gao, Z. Chen, A. Sun, and X. Deng, "Gender differences in cardiovascular disease," *Medicine in Novel Technology and Devices*, vol. 4, p. 100025, 2019.

[49] E. Schnabel, D. Nowak, S. Brasche, H.-E. Wichmann, and J. Heinrich, "Association between lung function, hypertension and blood pressure medication," *Respiratory medicine*, vol. 105, no. 5, pp. 727–733, 2011.

Peng Zhao received a bachelor's degree from Hefei University of Technology, where he is currently working toward the Ph.D. degree. He is currently working with the Anhui Province Key Laboratory of Affective Computing and Advanced Intelligent Machines, Hefei University of Technology, Hefei, China. His current research interests include intelligent information processing, wireless sensing, and machine learning.

Jinyang Huang received the Ph.D. degree in School of Cyberspace Security from the University of Science and Technology of China in 2022. He is currently a lecturer in the School of Computer and Information at Hefei University of Technology. His research interests include Wireless Security and Wireless Sensing. He is a TPC Member of ACM MM, IEEE ICME, and Globecom. He is now an editorial board member of Applied Sciences.

Xiang Zhang received the B.E. degree from Hefei University of Technology, China, in 2017, and his D.E. degree from the same university in 2023. Currently, he is a postdoc with the School of Cyber Science and Technology, University of Science and Technology of China. His research interests include wireless sensing and affective computing. He is a TPC Member of IEEE ICME and Globecom. He has served as a reviewer for IEEE TNNLS, TMM, and Pattern Recognition.

Zhi Liu (S'11-M'14-SM'19) received the Ph.D. degree in informatics in National Institute of Informatics. He is currently an Associate Professor at The University of Electro-Communications. His research interest includes video network transmission and mobile edge computing. He is now an editorial board member of Springer wireless networks and IEEE Open Journal of the Computer Society. He is a senior member of IEEE.

Yan Huan received the B.E. degree from Hefei University of Technology, China, in 2017, and his D.E. degree from the same university in 2023. He is currently a lecturer in the School of Big Data and Computer Science at Guizhou Normal University. His research interests include Wireless Security and Wireless Sensing.

Meng Wang received a bachelor's degree from Hefei University of Technology, where she is currently working toward the Ph.D. degree. She is currently working with the Anhui Province Key Laboratory of Affective Computing and Advanced Intelligent Machines, Hefei University of Technology, Hefei, China. Her current research interests include intelligent information processing, wireless sensing, and machine learning.

Guohang Zhuang graduated from Xinjiang University. Now a Ph.D. student at Hefei University of Technology, he currently focuses on intelligent perception, 3D object detection and emotional computing.

Yutong Guo He is currently working with the Anhui Province Key Laboratory of Affective Computing and Advanced Intelligent Machines, Hefei University of Technology, Hefei, China.

Xiao Sun was born in 1980. He received the M.E. degree from the Department of Computer Sciences and Engineering, Dalian University of Technology, Dalian, China, in 2004, the first Ph.D. degree from the University of Tokushima, Tokushima, Japan, in 2009, and the second Ph.D. degree Dalian University of Technology in 2010. He is currently working as an Professor with the Anhui Province Key Laboratory of Affective Computing and Advanced Intelligent Machines, Hefei University of Technology, Hefei, China. His research interests include affective computing, natural language processing, machine learning, and human–machine interaction.

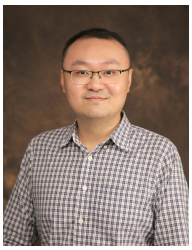

Meng Li is an Associate Professor and Dean Assistant at the School of Computer Science and Information Engineering, Hefei University of Technology (HFUT), China. He is also a Post-Doc Researcher at Department of Mathematics and HIT Center, University of Padua, Italy, where he is with the Security and PRIvacy Through Zeal (SPRITZ) research group led by Prof. Mauro Conti (IEEE Fellow). He obtained his Ph.D. in Computer Science and Technology from the School of Computer Science and Technology, Beijing Institute of Technology (BIT), China, in 2019. He was sponsored by ERCIM 'Alain Bensoussan' Fellowship Programme (from 2020.10.1 to 2021.3.31) to conduct Post-Doc research supervised by Prof. Fabio Martinelli at CNR, Italy. He was sponsored by China Scholarship Council (CSC) (from 2017.9.1 to 2018.8.31) for joint Ph.D. study supervised by Prof. Xiaodong Lin (IEEE Fellow) in the Broadband Communications Research (BBCR) Lab at University of Waterloo and Wilfrid Laurier University, Canada. His research interests include data security, privacy preservation, applied cryptography, blockchain, TEE, and Internet of Vehicles. In this area, he has published 70 papers in international peer-reviewed journals and conferences, including TIFS, TDSC, ToN, TKDE, TODS, TSC, TSG, TII, TVT, TNSM, TNSE, TGCN, COMST, MobiCom, ICICS, SecureComm, TrustCom, and IPCCC. He is a Senior Member of IEEE. He is an Associate Editor for IEEE TIFS, IEEE TNSM, and IEEE IoTJ.